Detection of Background Water Leaks Using a High-Resolution Dyadic Transform

Eduardo Trutié-Carrero [1], Diego Seuret-Jiménez [1,*], José M. Nieto-Jalil [2,*], Julio C. Herrera-Díaz [1], Jorge Cantó [3] and J. Jesús Escobedo-Alatorre [1]

1 Centro de Investigación en Ingeniería y Ciencias Aplicadas, Universidad Autónoma del Estado de Morelos, Ave. Universidad 1001, Cuernavaca 62209, Mexico
2 Tecnologico de Monterrey, School of Engineering and Sciences, Reserva Territorial Atlixcáyotl, Puebla 72453, Mexico
3 Corrosión y Protección (CyP), Buffon 46, Mexico City 11590, Mexico
* Correspondence: dseuret@uaem.mx (D.S.-J.); jnietoj@tec.mx (J.M.N.-J.)

Abstract: This article solves the problem of detecting water leaks with a minimum size of down to 1 mm in diameter. Two new mathematical tools are used to solve this problem: the first one is the $\mathcal{T}_e$ cross-spectral density and the second is $\mathcal{T}_e$ coherence. These mathematical tools provide the possibility of discriminating spurious frequency components, making use of the property of multi-sensitivity. This advantage makes it possible to maximize the sensitivity of the frequency spectrum. The wavelet function used was Daubechies 45, because it provides an attenuation of 150 dB in the rejection band. The tools were validated with two scenarios. For the first scenario, a synthetic signal was analyzed. In the second scenario, two types of background leakage were analyzed: the first one has a diameter of 1 mm with a signal-to-noise ratio of 2.82 dB and flow rate of 33.7 mL/s, and the second one has a diameter of 4 mm with a signal-to-noise ratio of 9.73 dB with a flow rate of 125.0 mL/s. The results reported in this paper show that both the $\mathcal{T}_e$ cross-spectral density and $\mathcal{T}_e$ coherence are higher than those reported in scientific literature.

Keywords: cross-correlation; frequency dyadic spectrum; $\mathcal{T}_e$ coherence; $\mathcal{T}_e$ cross-spectral density; $\mathcal{T}_e$ transform

1. Introduction

This paper shows a feature extraction study of water leaks with a diameter of 1 mm and 4 mm, in a controlled laboratory environment. This study makes use of the $\mathcal{T}_e$ transform [1] and its properties in the frequency domain.

Nowadays, one of the most widely used approaches in pipeline fault feature extraction is performed in the domain of frequency [2–4]. This is because the frequency domain reveals characteristics of the signal to be analyzed that are not visible in the time domain. For this reason, this article shows two new mathematical tools for extracting the characteristics of a signal in the frequency domain:

1. The first is the $\mathcal{T}_e$ cross-spectral density.
2. The second is $\mathcal{T}_e$ coherence.

These mathematical tools are based on the $\mathcal{T}_e$ transform [1] and in the cross-correlation function [5–8]. The main objective of this new approach increases sensitivity in the frequency spectrum. This makes it possible to detect water leaks of a small size. These contributions were validated by the behavior of a pipeline with two types of background leakage, the first with a diameter of 1 mm and the second with a diameter of 4 mm.

There is currently great interest in detecting non-catastrophic background leaks with a flow rate below the limit commonly known as Unavoidable Annual Real Losses [9,10]. There is interest in background leaks with these characteristics since they are precursors to catastrophic water leaks.

The authors of [8,11] state that these losses are due to a variety of factors. These include demographic, socioeconomic, and environmental factors, such as rapid population growth, rapid urbanization, unsustainable consumption patterns, and groundwater and surface water pollution. The authors in [12] reveal that these problems are compounded by events arising from operations, such as turning pumps on or off and opening or closing valves. Some of these events are aggravated by the aging and corrosion of these installations, leading to background water leaks that increase repair costs.

Due to the adversities caused by water leaks, it is of great interest to minimize the life span, which begins when this event is generated and ends when the water distribution system comes to repair it. This problem has motivated many researchers to study and propose different solutions in the frequency domain for background leakage.

In [13], the authors carried out work aimed at detecting water leaks in plastic pipes. In this work, they use the Fourier transform, the short-time Fourier transform, and the continuous Wavelet transform to detect the presence of leakage. In addition, they analyze leaks with a diameter of 6 mm and 10 mm. In the research reported by [14], the vibroacoustic characteristics of leakage in buried water pipes were studied. After conducting their study, they propose that before processing the cross-correlation function, unwanted noise should be removed. This is achieved by filtering the data in a frequency bandwidth where there is leakage information. In addition, they use cross-spectral density and coherence to extract the background leakage feature.

Researchers in [15] investigated to detect background leakage, under controlled conditions, with a flow rate of 0.6 L/min. To solve their problem, they use power spectral density. Authors in [16] performed work on the influence of piping material on the background leakage signal for real and complex water distribution systems. In the work of [17], the process of differentiation is applied in urban pipeline networks to detect leaks based on correlation. For this purpose, the authors use cross-spectral density.

In [9], they present a work directed towards the study of vibrations to detect water leaks. In that article, the authors use auto-correlation analysis and power spectral density to extract the water leakage feature. In the study shown in [18], they analyze the detection of background leakage in water pipelines under a noisy environment. For their study, these authors considered that in practice, leakage signals coexist with white noise and color noise. They used the coherence function and cross-spectral density for their analysis.

The article [19] shows a study for detecting water leaks in a steam generator. The authors use cross-spectral density to analyze the background leakage generated. The research of [20] shows a work aimed at leak detection in urban water distribution systems, where a study is conducted on the accuracy of different technologies in the detection of background leaks. In said study, the authors did not detect any leaks below the limit commonly known as Unavoidable Annual Real Losses [10]. The authors of [21] show a procedure based on linear prediction for leak detection in water distribution networks. For their analysis, they used the short-time Fourier transform.

Despite the existing advantages of the mathematical methods reported in the scientific literature, the main drawback is that there is no mathematical tool to calculate cross-spectra. This maximizes the sensitivity of the frequency spectrum and in parallel makes it possible to extract background leakage characteristics below the limit commonly known as Unavoidable Annual Real Losses.

For this reason, to find new study methods that do not exist in the international literature, this manuscript proposes two new mathematical tools to calculate crossed spectra. The first contribution is the $\mathcal{T}_e$ cross-spectral density and the second contribution is $\mathcal{T}_e$ coherence. Our results show the possibility of characterizing, in the dyadic frequency domain, background leakage generated in a controlled laboratory environment corresponding to 1 mm and 4 mm leakage.

The remainder of the article is organized as follows. Section 2 presents the theoretical background for $\mathcal{T}_e$ cross-spectral density and $\mathcal{T}_e$ coherence. Section 3 shows the contributions to the knowledge presented in this article, which are $\mathcal{T}_e$ cross-spectral density and $\mathcal{T}_e$

coherence. Section 4 shows the experimental setup used. Section 5 shows the simulation and experimental results together with discussions. Finally, the main conclusions are shown in Section 6.

2. Theoretical Background

In this section, we describe the theoretical bases used to obtain the $\mathcal{T}_e$ cross-spectral density and $\mathcal{T}_e$ coherence. The authors start with the definition of the cross-correlation function, and then with the definition of the $\mathcal{T}_e$ transform. Subsequently, with the definition of the cross-spectral density function, and finally with the definition of the coherence function.

2.1. Cross-Correlation Function

The cross-correlation function is widely used in fault detection [22–24] to extract features that highlight the relationship between two signals.

If there are two signals $x_1(t), x_2(t) \in L^1(\mathbb{R}) \ \forall \ t \in \mathbb{R}$ stationary and ergodic, then the cross-correlation function is defined by [25,26] as shown in Equation (1).

$$R_{x_1,x_2}(\tau) = E[x_1(t)x_2(t+\tau)] \tag{1}$$

where $\tau \in \mathbb{R}$ and indicates the delay between $x_1(t)$ and $x_2(t)$, E is the expected value operator.

To perform an easy-to-interpret feature extraction, it is very useful to express the cross-correlation in a normalized form, giving Equation (1) as expressed in Equation (2),

$$\rho_{x_1,x_2}(\tau) = \frac{R_{x_1,x_2}(\tau)}{\sqrt{R_{x_1,x_1}(0)R_{x_2,x_2}(0)}} \tag{2}$$

where $R_{x_1,x_1}(0)$ is the auto-correlation function for x_1, $R_{x_2,x_2}(0)$ is the auto-correlation function for x_2, $-1 \leq \rho_{x_1,x_2}(\tau) \leq 1$, indicating that 0 and ± 1 are minimum and maximum correlation, respectively.

2.2. $\mathcal{T}_e$ Transform

The $\mathcal{T}_e$ transform defined by [1] is a mathematical tool that allows for obtaining a dyadic frequency spectrum. Its main advantage is that it allows the isolation of spurious frequency components.

If $f(t) \in L^1(\mathbb{R}) \ \forall \ t \in \mathbb{R}$ then the $\mathcal{T}_e$ transform is defined by [1] as shown in Equation (3).

$$\widehat{f}_{DTe}[f(t)](\mu, \xi, \vartheta) = \int_{-\infty}^{\infty} f(t)g^*_{\mu,\xi,\vartheta}(t)dt \qquad \forall \, \mu, \xi, \, \vartheta \in \mathbb{Z}^+ \tag{3}$$

where $\widehat{f}_{DTe}[f(t)](\mu, \xi, \vartheta)$ are the $\mathcal{T}_e$ coefficients of $f(t)$, $g^*_{\mu,\xi,\vartheta}(t) = w^*_\mu(t)\psi^*_{\xi,\mu}(t)e^{-i2\pi\vartheta t}$ is kernel $\mathcal{T}_e$, $w^*_\mu(t) = w^*(t-\mu) \in L^1(\mathbb{R}) \cap L^2(\mathbb{R})$ is a window function, $\psi^*_{\xi,\mu}(t) = \frac{1}{\sqrt{2^\xi}}\psi^*\left(2^{-\xi}t - \mu\right) \in L^1(\mathbb{R}) \cap L^2(\mathbb{R})$ is a dyadic wavelet function, and 2^ξ and μ are the scaling and translation parameters, respectively.

2.3. Cross-Spectral Density Function

Cross-spectral density is a mathematical tool widely used in the field of fault detection because it allows us to know, in the frequency spectrum, the relationship between two signals [27–29].

This function is based on calculating the Fourier transform of the cross-correlation function described in Equation (1). Equation (4) defines the cross-spectral density for $x_1(t), x_2(t) \in L^1(\mathbb{R}) \ \forall \ t \in \mathbb{R}$ [30,31].

$$S_{x_1,x_2}(\omega) = \int\limits_{-\infty}^{\infty} R_{x_1,x_2}(\tau)e^{-i\omega\tau}d\tau \tag{4}$$

2.4. Coherence Function

Coherence is a particular case of cross-spectral density. The main advantage of this function is that it normalizes the relationship between two signals, $x_1(t), x_2(t) \in L^1(\mathbb{R}) \; \forall \; t \in \mathbb{R}$, in the frequency domain. This advantage has led this function to be widely used in the area of fault detection [32–34]. Equation (5) defines the coherence function [31].

$$G_{x_1,x_2}(\omega) = \frac{|S_{x_1,x_2}(\omega)|}{\sqrt{S_{x_1,x_1}(\omega)S_{x_2,x_2}(\omega)}} \tag{5}$$

where $S_{x_1,x_1}(\omega)$ is the auto-spectrum of $x_1(t)$, $S_{x_2,x_2}(\omega)$ is the auto-spectrum of $x_2(t)$, and $0 \leq G_{x_1,x_2}(\omega) \leq 1$, indicating that zero and one are minimum and maximum coherence, respectively.

3. Method for the Detection of Water Background Leakage

In this section, the authors show the main contributions to this work. It is important to note that the mathematical basis for these contributions was presented in the previous section (Section 2).

Signal analysis using the cross-spectral approach has been of great importance in several areas of knowledge [35–37]. Among the works reported, a focus on the continuous Wavelet transform is found [38–41]. Despite the progress achieved, its main drawback is that it does not allow multiple-resolution analysis using a dyadic approach. This makes it impossible to isolate frequency components that are not characteristic of the system to be analyzed.

To solve this problem, the authors of this paper show, in Sections 3.1 and 3.2, new study methods not existing in the international literature for the detection of background water leakage. The main advantage of these mathematical tools is that they allow the investigation of the relationship between two signals in the dyadic frequency spectrum.

Section 3.1 shows $\mathcal{T}_e$ cross-spectral density and Section 3.2 $\mathcal{T}_e$ coherence.

3.1. $\mathcal{T}_e$ Cross-Spectral Density Function

This subsection shows the first contribution aimed at obtaining a function defining the $\mathcal{T}_e$ cross-spectrum, through the cross-correlation link and the $\mathcal{T}_e$ transform.

The $\mathcal{T}_e$ cross-spectrum provides a dyadic cross-spectrum that allows extraction of characteristics of systems under deterministic or stochastic processes, increasing the sensitivity of the frequency spectrum.

If we replace the $f(t)$ signal of Equation (3) with cross-correlation, $R_{x_1,x_2}(\tau)$, defined in Equation (1) we obtain Equation (6) which defines the $\mathcal{T}_e$ cross-spectral density. It is important to note that Equation (6) is defined for two signals $x_1(t), x_2(t) \in L^1(\mathbb{R}) \; \forall \; t \in \mathbb{R}$.

$$\widehat{Y}_{x_1,x_2}(\mu,\xi,\vartheta) = \int\limits_{-\infty}^{\infty} R_{x_1,x_2}(\tau)g^*_{\mu,\xi,\vartheta}(\tau)d\tau \qquad \forall \; \mu,\xi,\;\vartheta \in \mathbb{Z}^+ \tag{6}$$

where $\widehat{Y}_{x_1,x_2}(\mu,\xi,\vartheta)$ is $\mathcal{T}_e$ cross-spectral density.

3.2. $\mathcal{T}_e$ Coherence Function

This subsection shows the second contribution of this manuscript, which is based on the first contribution shown in Section 3.1. This is oriented to obtain the particular case of the $\mathcal{T}_e$ cross-spectral density, which is $\mathcal{T}_e$ coherence.

$\mathcal{T}_e$ coherence is obtained by normalizing Equation (6) by the $\mathcal{T}_e$ auto-spectra of the signals $x_1(t)$ and $x_2(t)$. Equation (7) defines the $\mathcal{T}_e$ coherence function for signals $x_1(t)$ and $x_2(t)$.

$$\Omega_{x_1,x_2}(\mu,\xi,\vartheta) = \frac{\left|\widehat{Y}_{x_1,x_2}(\mu,\xi,\vartheta)\right|}{\sqrt{\left|\widehat{Y}_{x_1,x_1}(\mu,\xi,\vartheta)\right|\left|\widehat{Y}_{x_2,x_2}(\mu,\xi,\vartheta)\right|}} \tag{7}$$

where $\left|\widehat{Y}_{x_1,x_1}(\mu,\xi,\vartheta)\right|$ is the absolute value of the $\mathcal{T}_e$ auto-spectrum of $x_1(t)$, $\left|\widehat{Y}_{x_2,x_2}(\mu,\xi,\vartheta)\right|$ is the absolute value of the $\mathcal{T}_e$ auto-spectrum of $x_2(t)$, and $0 \leq \Omega_{x_1,x_2}(\mu,\xi,\vartheta) \leq 1$, indicating that 0 and 1 are the minimum and maximum $\mathcal{T}_e$ coherence, respectively.

4. Experimental Design

To validate the two contributions, an installation consisting of a slightly rusted cast iron pipe with a length of 90 cm and an outer and inner diameter of 8.5 cm and 8.2 cm, respectively, was used.

The distance between the sensors is d $= 30$ cm and the distance from each sensor to the leakage is 15 cm. In addition, 2 scenarios were used: In the first one, two simulated signals were used with the addition of white Gaussian additive noise. In the second scenario, two background leaks were generated, a 1 mm and an 4 mm in diameter background leak. Figure 1 shows the schematic of the installation used for background leak detection. Note, in this figure, how the position of the sensors is described, highlighting the distance between them and the distance from each sensor to the background leakage.
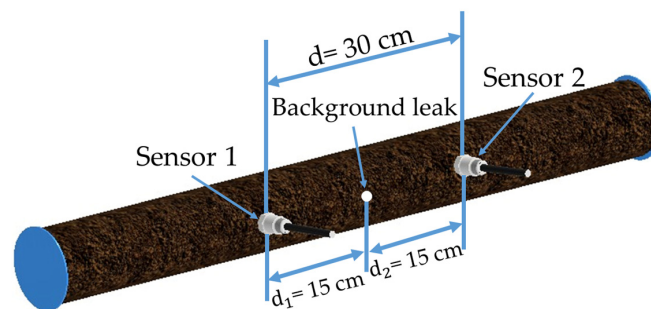
Figure 1. Scheme for background leakage detection.

The data acquisition process used two 603C01 uniaxial piezoelectric accelerometers, which have a sensitivity of 100 mV/g and a dynamic range of ± 50 g. A data acquisition system was also used from National Instrument NI 9234 and NIcDAQ $- 9172$ together with the LabView (2018 version) program. The vibration signals were sampled in compliance with Nyquist's theorem. A sampling frequency of 500 Hz was used since leakage has components with frequencies lower than 250 Hz. Experiments were conducted at room temperature (25 °C) and atmospheric pressure (1019 hPa).

5. Results and Discussion

The objective of this section is to present the advantages of the contributions of this article (see Section 3) compared to those reported by the scientific community (see Sections 2.3 and 2.4).

For this reason, the authors of this paper divided Section 5 into two subsections. Section 5.1 shows the results obtained under a simulation environment. Section 5.2 shows the results achieved for two different background leakages under a real controlled experimental environment. In signal processing with $\mathcal{T}_e$ cross-spectral density and $\mathcal{T}_e$ coherence, the Hamming function was used as a window and the Daubechies 45 as a wavelet. The Daubechies 45 was selected because it provides an attenuation of 150 dB in the rejection band [42].

5.1. Simulated Signal Scenario

In this first scenario, the authors show the simulation results obtained with the procedures reported in the scientific community and the two contributions reported in this article.

The main objective of this subsection is to show from a deterministic approach the effectiveness of the contributions shown in Section 3 in comparison with the procedures reported in the literature.

To obtain the results shown in this subsection, two signals were simulated with the presence of additive white Gaussian noise: The first signal has frequency components of 10 Hz and 100 Hz. The second one presents frequency components of 50 Hz and 100 Hz.

Figures 2 and 3 show the results obtained by the cross-spectral density function and the coherence function, respectively. Note, in these figures, how it is possible to extract the 100 Hz frequency characteristic, discriminating the frequency components that are not equal. On the other hand, note, how from Figures 4–7, it can be observed that both the $\mathcal{T}_e$ cross-spectral density as well as the $\mathcal{T}_e$ coherence add the advantage of isolating the 100 Hz frequency component between the two analysis signals. However, it maintains the advantage of discriminating frequency components that are not common. This advantage makes it possible to analyze, on a specific scale, a frequency component without the intervention of frequency components that do not correspond to the background leakage being analyzed.
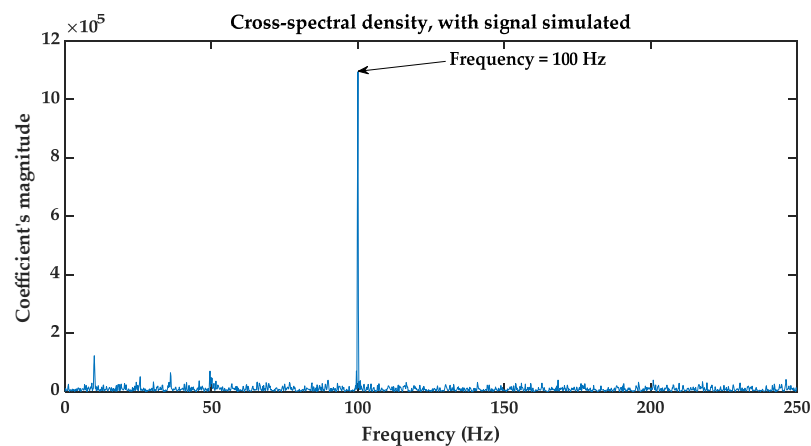
Figure 2. Cross-spectral density, with two synthetic signals: $S_1 = sin(2\pi 10t) + sin(2\pi 100t)$ and $S_1 = sin(2\pi 50t) + sin(2\pi 100t)$.
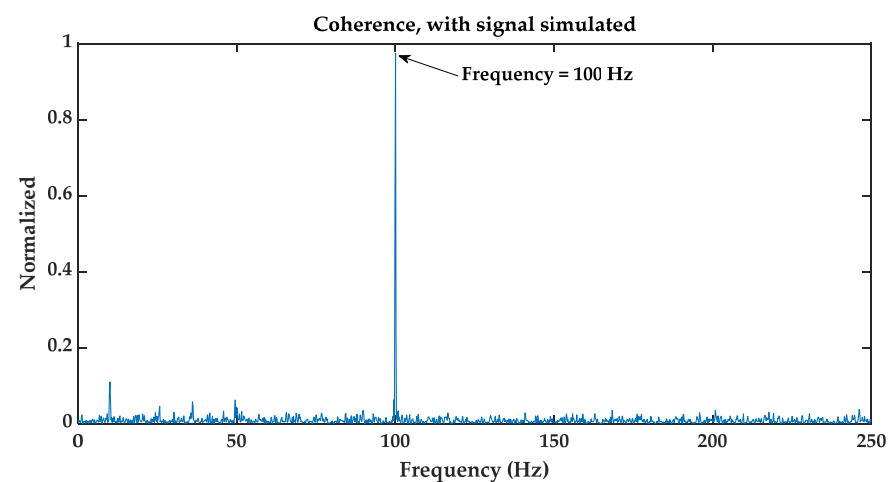
Figure 3. Coherence, with two synthetic signals: $S_1 = sin(2\pi 10t) + sin(2\pi 100t)$ and $S_1 = sin(2\pi 50t) + sin(2\pi 100t)$.
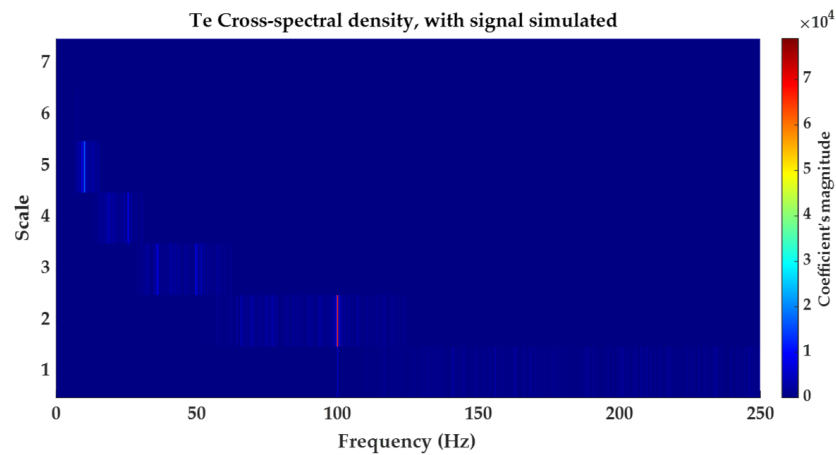
Figure 4. $\mathcal{T}_e$ cross-spectral density, with two synthetic signals: $S_1 = sin(2\pi10t) + sin(2\pi100t)$ and $S_1 = sin(2\pi50t) + sin(2\pi100t)$.
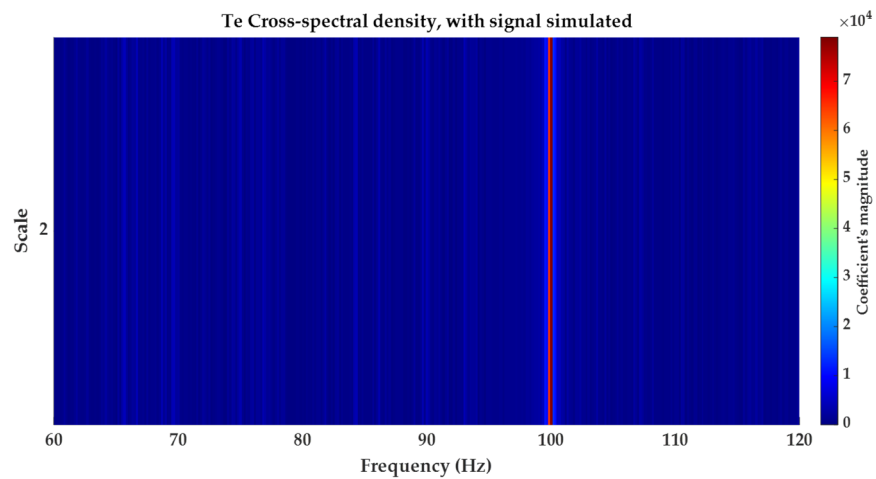
Figure 5. $\mathcal{T}_e$ cross-spectral density in Scale 2, with two synthetic signals: $S_1 = sin(2\pi10t) + sin(2\pi100t)$ and $S_1 = sin(2\pi50t) + sin(2\pi100t)$. Absolute error $1 * 10^{-3}$.
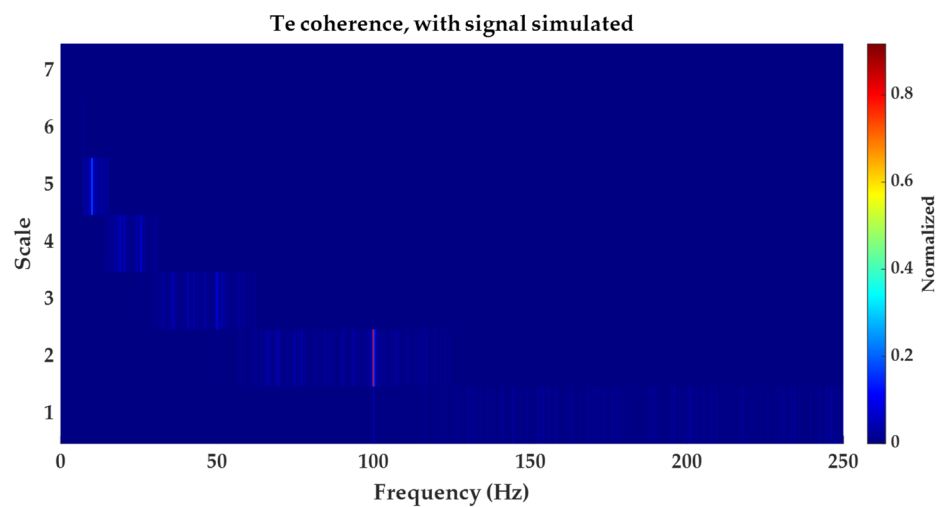
Figure 6. $\mathcal{T}_e$ coherence, with two synthetic signals: $S_1 = sin(2\pi10t) + sin(2\pi100t)$ and $S_1 = sin(2\pi50t) + sin(2\pi100t)$.
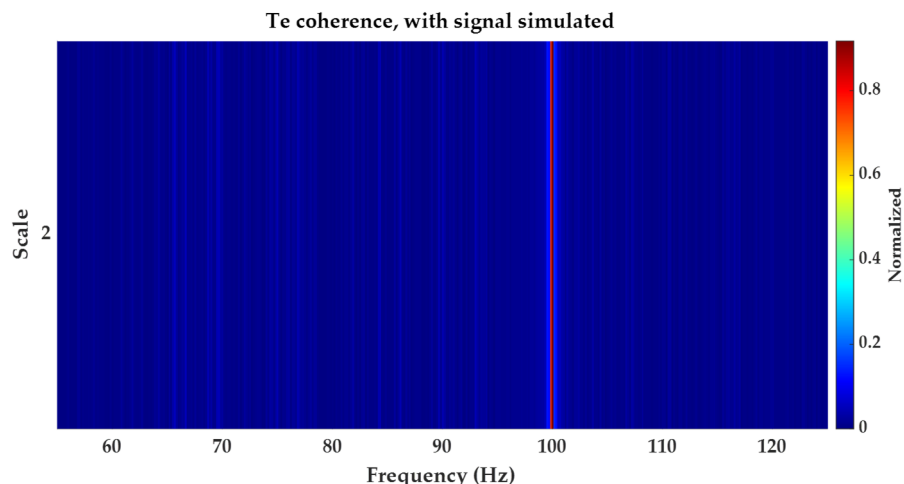
Figure 7. $\mathcal{T}_e$ coherence in Scale 2, with two synthetic signals: $S_1 = sin(2\pi10t) + sin(2\pi100t)$ and $S_1 = sin(2\pi50t) + sin(2\pi100t)$. Absolute error $1 * 10^{-3}$.

5.2. Real Experimentation Scenarios

In this subsection, the authors validate, through real experiments, the contributions shown in Section 3. For this, they used a scenario under the setup shown in Section 4. The said scenario was used to analyze two types of background leakage. The first background leak is 1 mm in diameter with a signal-to-noise ratio of 2.82 dB and a flow rate of 33.7 mL/s. The second background leak is 4 mm in diameter with a signal-to-noise ratio of 9.73 dB and a flow rate of 125.0 mL/s. Figures 8 and 9 show the signals corresponding to sensors 1 and 2, respectively. Notice, in these figures, how the amplitude of the background leak corresponding to 1 mm of diameter and the amplitude of the signal without background leak are very close. This highlights the need to analyze background leakage signals with mathematical tools that allow analyzing such signals through their frequency characteristics.
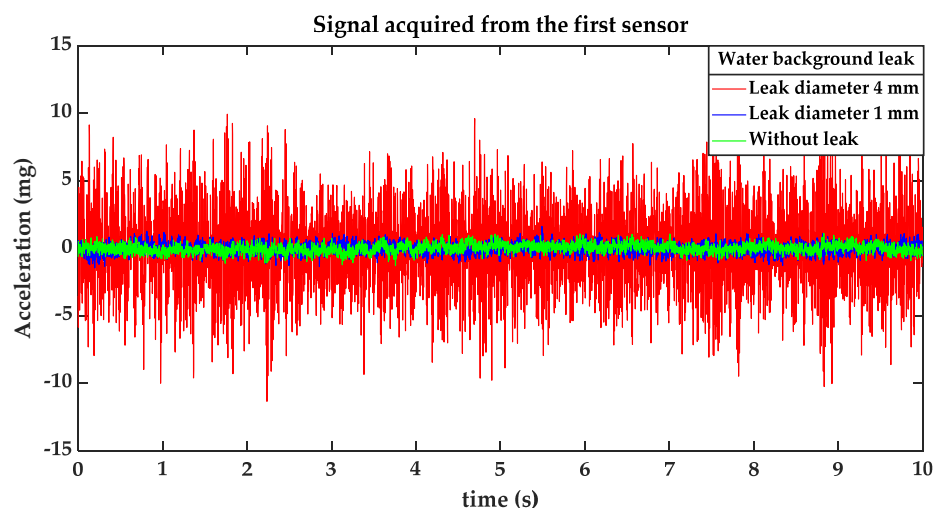
Figure 8. Signals were acquired from the first sensor with a background leak of 1 mm and 4 mm in diameter.
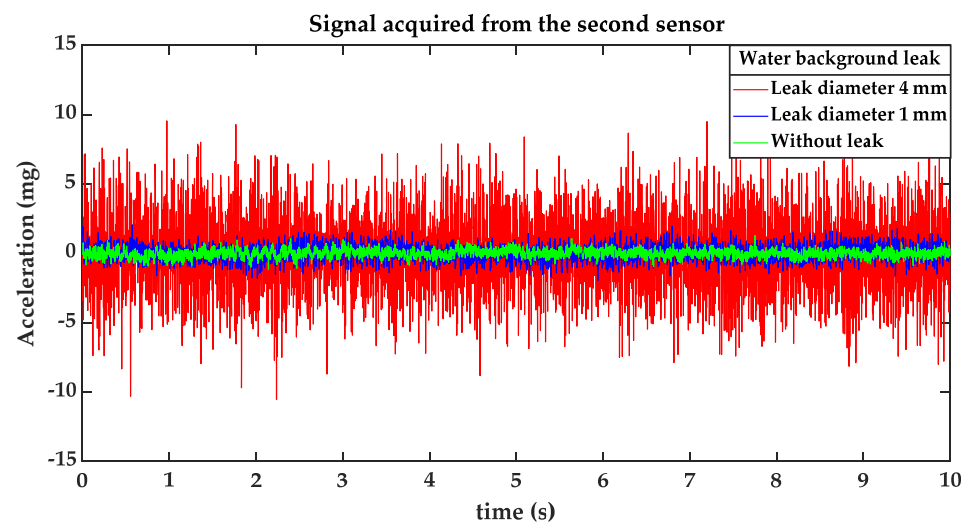
Figure 9. Signals were acquired from the second sensor with a background leak of 1 mm and 4 mm in diameter.

5.2.1. Results Obtained for Background Leakage of 1 mm in Diameter

This subsubsection shows the results obtained after processing the signals displayed in Figures 8 and 9. Note that for Figures 10 and 11, as well as for the leakage of 1 mm in diameter, two frequency components appear (17.0 Hz and 31.7 Hz), which are apparently associated with the background leakage. On the other hand, notice how in Figure 11, the coherence obtained is less than 0.6, which indicates that there is a very poor relation between the signals arriving at the sensors. This result is because the signal related to the 1 mm background leakage has a signal-to-noise ratio close to the noise floor of the data acquisition system, which causes the signal to be very weak at the reception point, making the feature extraction process difficult.
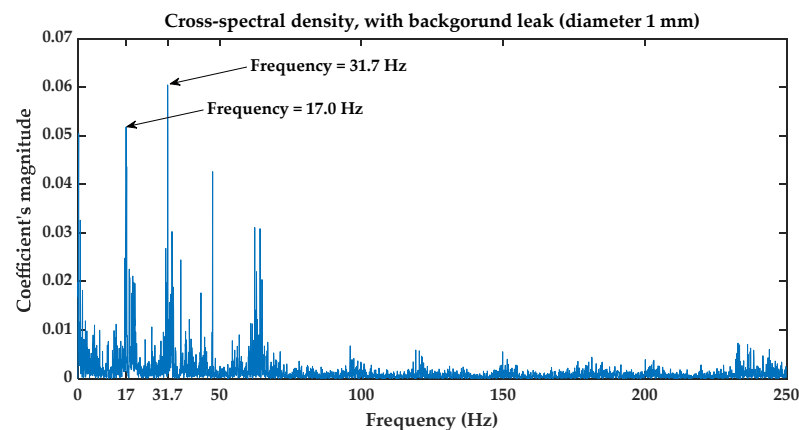
Figure 10. Cross-spectral density, with background leak (1 mm in diameter) and flow rate 33.7 mL/s.

However, the results are shown by the $\mathcal{T}_e$ cross-spectral density (see Figures 12–14) and $\mathcal{T}_e$ coherence (see Figures 15 and 16) show superiority over the above-mentioned procedures. Notice how both the $\mathcal{T}_e$ cross-spectrum and the $\mathcal{T}_e$ coherence highlight the frequency component related to background leakage. This result is due to the fact that these contributions are based on showing a dyadic frequency spectrum that allows obtaining multi-sensitivity in the frequency spectrum, which allows detection of background leakage of 1 mm in diameter.
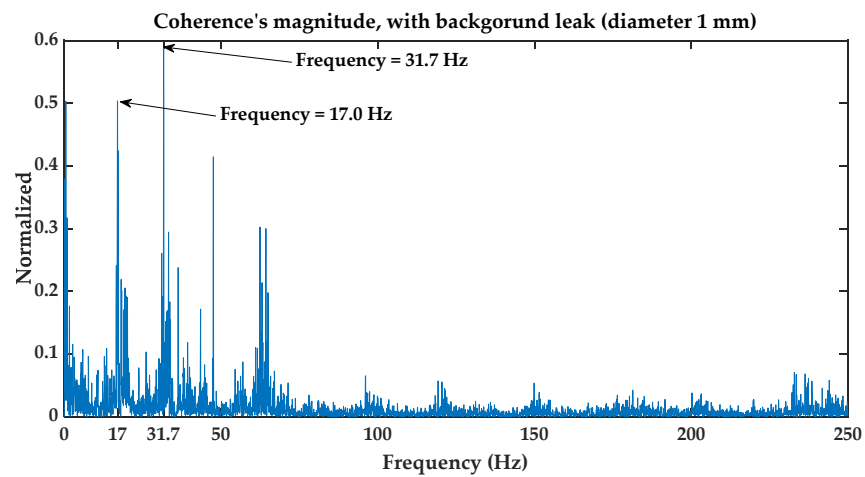
Figure 11. Coherence's magnitude, with background leak (1 mm in diameter) and flow rate 33.7 mL/s.
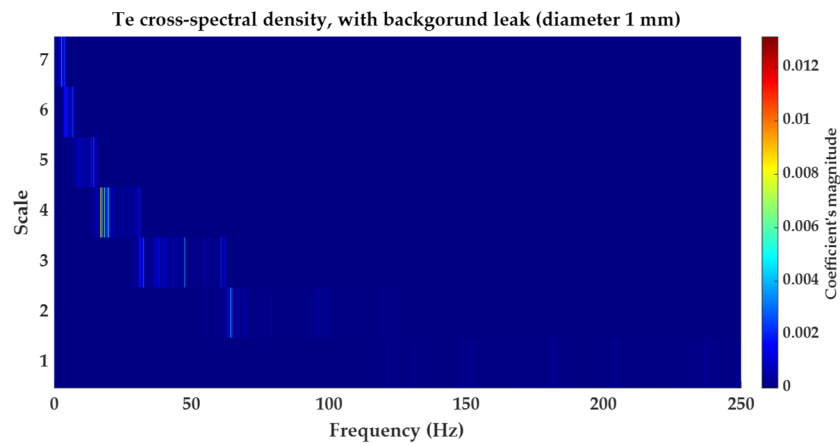
Figure 12. $\mathcal{T}_e$ cross-spectral density, with background leak (1 mm in diameter) and flow rate 33.7 mL/s.
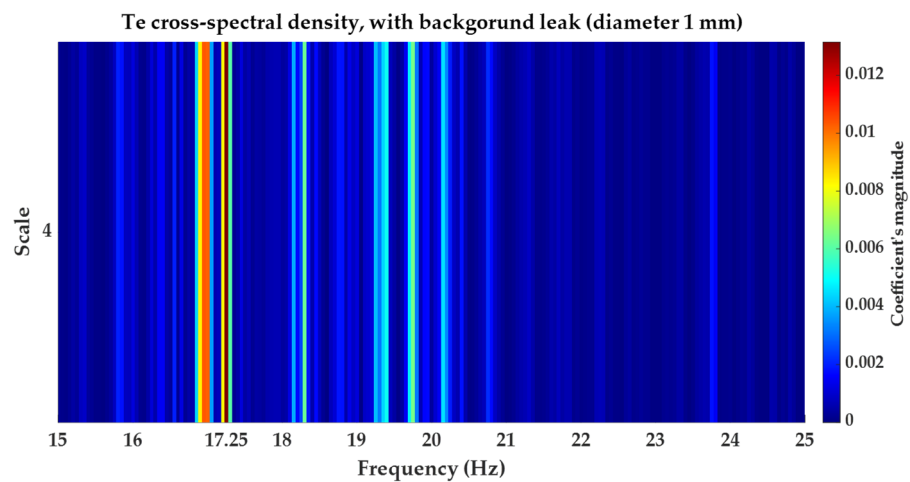
Figure 13. $\mathcal{T}_e$ cross-spectral density in Scale 4, with background leak (1 mm in diameter) and flow rate 33.7 mL/s.
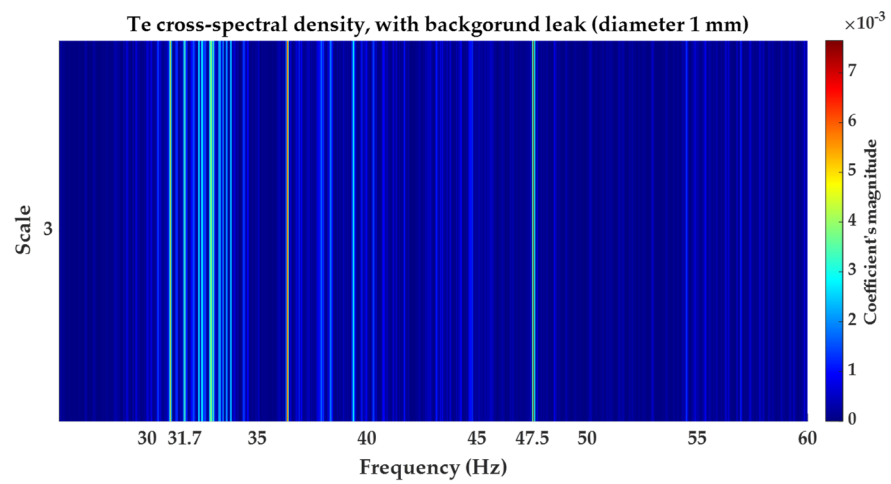
Figure 14. $\mathcal{T}_e$ cross-spectral density in Scale 3, with background leak (1 mm in diameter) and flow rate 33.7 mL/s.
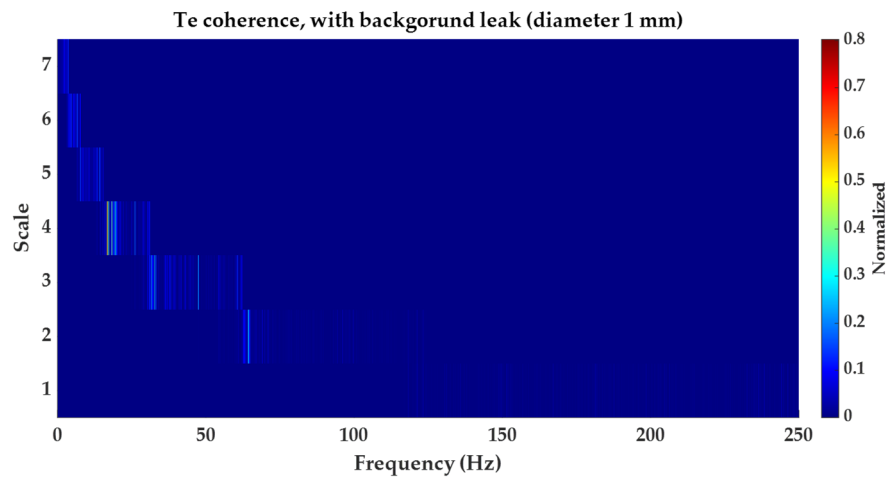
Figure 15. $\mathcal{T}_e$ coherence, with background leak (1 mm in diameter) and flow rate 33.7 mL/s.
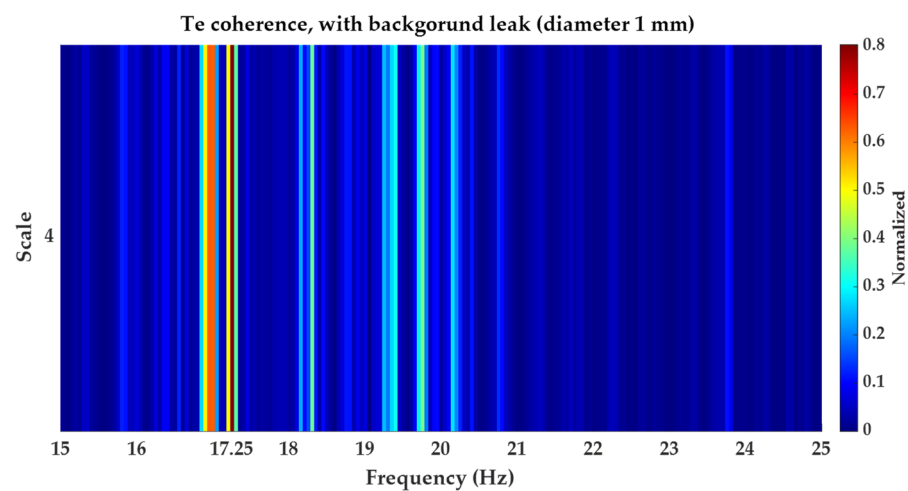
Figure 16. $\mathcal{T}_e$ coherence in Scale 4, with background leak (1 mm in diameter) and flow rate 33.7 mL/s.

Another important result is that the dyadic frequency spectrum obtained by the $\mathcal{T}_e$ cross-spectral density and $\mathcal{T}_e$ coherence discriminates frequency components corresponding to the color noise (31.7 Hz frequency component) as shown in Figure 14. This property

allows highlighting only the frequency component related to background leakage. This result is observed when comparing Figures 10–16.

5.2.2. Results Obtained for Background Leakage of 4 mm in Diameter

This section shows the results obtained after processing the acquired signals of 4 mm diameter background leakage (see Figures 8 and 9).

Figures 17 and 18 show the results obtained by cross-spectral density and coherence, respectively. Note that in this case, the background leakage has a frequency component of 86.36 Hz.
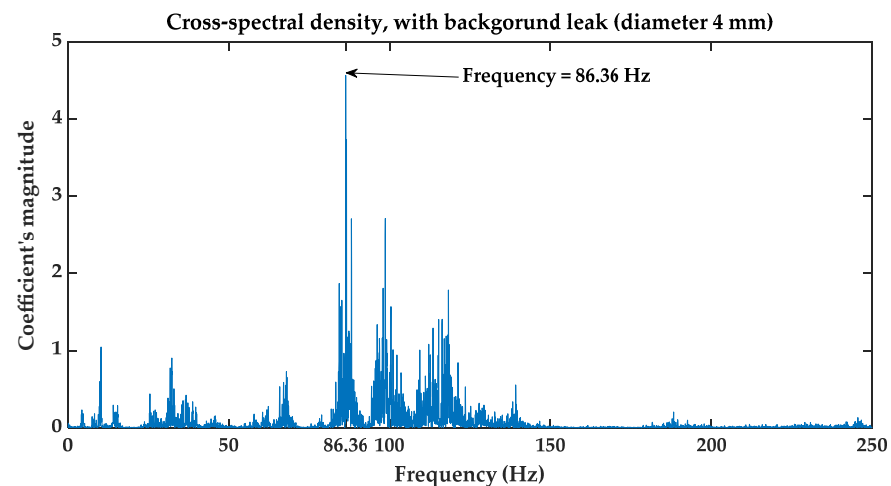
Figure 17. Cross-spectral density, with background leak (4 mm in diameter) and flow rate 125.0 mL/s.
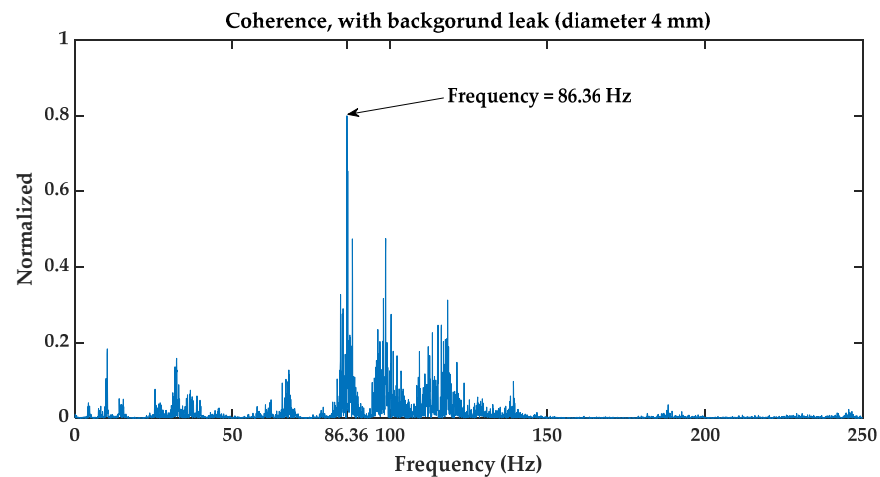
Figure 18. Coherence, with background leak (4 mm in diameter) and flow rate 125.0 mL/s.

Notice how even though this type of leak has a higher signal-to-noise ratio than the 1 mm diameter leak, the sensitivity of the frequency spectrum is maximized with the contributions shown in this article.

Figures 19–22 show the result obtained after computing the $\mathcal{T}_e$ cross-spectral density and $\mathcal{T}_e$ coherence. Observe in these figures how different frequency bands appear where spurious frequencies are observed. If we focus only on scale 2, we can see that this is where the frequency component with the highest density is concentrated. This allows us to characterize the frequency component of the background leakage. This provides the possibility of extracting the background leakage characteristic with maximum accuracy. This is shown by comparing the results displayed in Figures 17 and 18 with those shown in Figures 20 and 22.
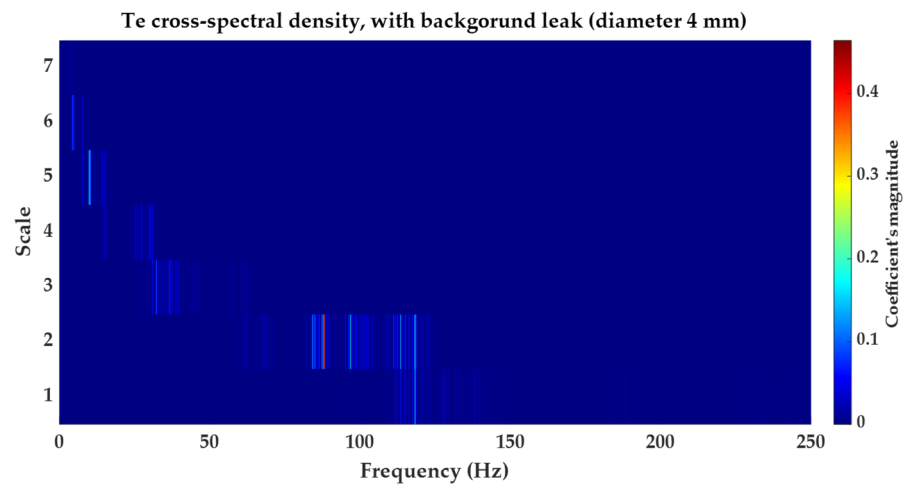
Figure 19. $\mathcal{T}_e$ cross-spectral density, with background leak (4 mm in diameter) and flow rate 125.0 mL/s.
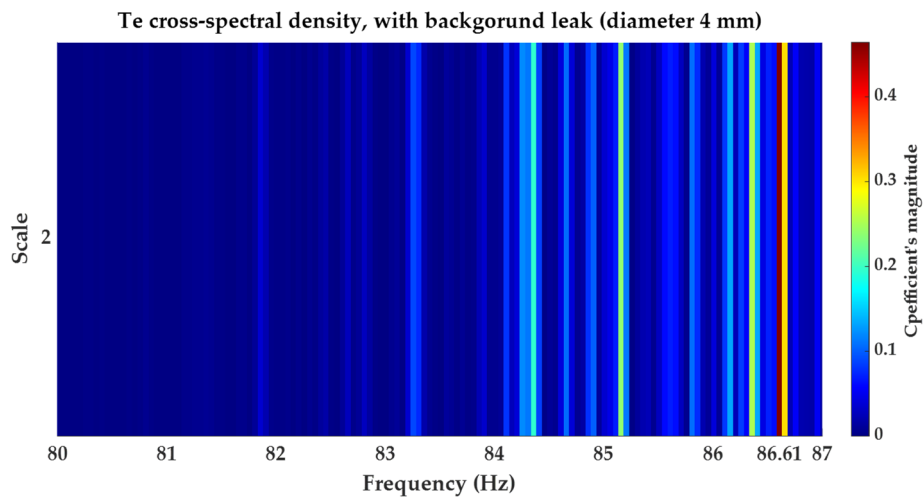
Figure 20. $\mathcal{T}_e$ cross-spectral density in Scale 2, with background leak (4 mm in diameter) and flow rate 125.0 mL/s.
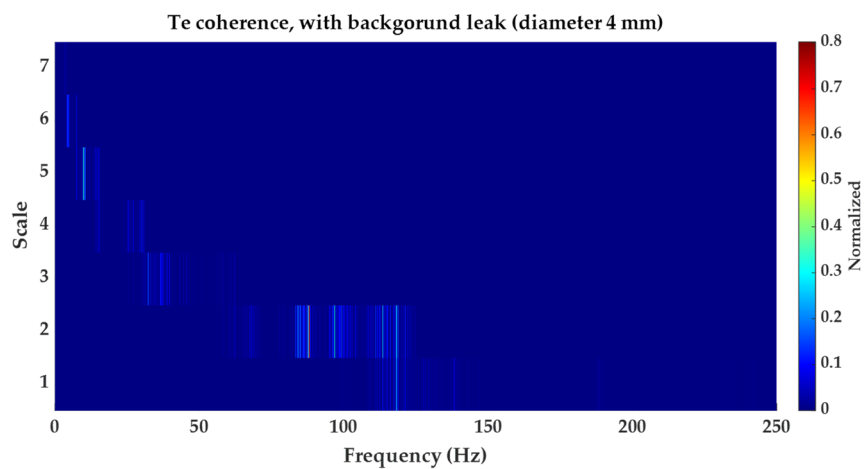
Figure 21. $\mathcal{T}_e$ coherence, with background leak (4 mm in diameter) and flow rate 125.0 mL/s.
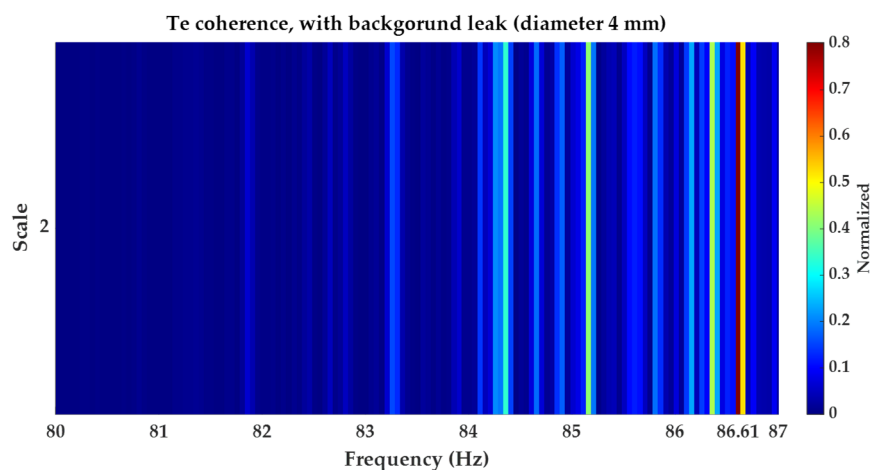
Figure 22. $\mathcal{T}_e$ coherence in Scale 2, with background leak (4 mm in diameter) and flow rate 125.0 mL/s.

These contributions allow the investigation of the relationship between two signals in the dyadic frequency domain. The main advantage they present is that they allow the extraction of the common frequency characteristic between two signals by discriminating the frequency components that correspond to color noise.

6. Conclusions

This paper presented two contributions based on the link of the $\mathcal{T}_e$ transform and the cross-correlation function, to detect background leakage of down to 1 mm diameter and flow rate of 33.7 mL/s. The first contribution is the $\mathcal{T}_e$ cross-spectral density and the second contribution is $\mathcal{T}_e$ coherence.

The detection of such small leaks provides great strength to the water distribution systems in knowing the current state of the distribution network. Which makes such leaks a precursor to catastrophic water leaks.

The results obtained show that the two contributions presented in this paper are superior to the state-of-the-art procedures that have previously been reported in the literature. This is because the procedures reported in the scientific literature are not able to extract the frequency component of the background leakage by isolating it from the spurious components. In addition, the procedures reported in the literature lack sensitivity in the frequency spectrum.

In future work, we will focus on the study of the properties of the $\mathcal{T}_e$ cross-spectral density and $\mathcal{T}_e$ coherence. We will also evaluate their performance in a real, uncontrolled environment. In addition, we will work on the implementation of the the $\mathcal{T}_e$ cross-spectral density and the $\mathcal{T}_e$ coherence in environments such as those provided by EPANET, allowing researchers to analyze the frequency components of background water leaks.

Author Contributions: Conceptualization, E.T.-C.; Supervision, D.S.-J.; Formal analysis, J.M.N.-J.; Validation J.C.H.-D.; Investigation J.C.; Investigation J.J.E.-A. All authors have read and agreed to the published version of the manuscript.

Funding: This research received no external funding.

Data Availability Statement: Data are not available due to ethical or privacy restrictions.

Acknowledgments: The authors thank H. Seuret-Silva for the technical support in reviewing the manuscripts. The work described in this paper is supported by CONACYT, Mexico.

Conflicts of Interest: The authors declare no conflict of interest concerning the publication of this manuscript.

References

1. Trutié-Carrero, E.; Seuret-Jimenez, D.; Nieto-Jalil, J.M. A high-resolution dyadic transform for non-stationary signal analysis. *Mathematics* **2021**, *9*, 3041. [CrossRef]
2. Bang, S.S.; Lee, Y.H.; Shin, Y.J. Defect detection in pipelines via guided wave-based time-frequency-domain reflectometry. *IEEE Trans. Instrum. Meas.* **2021**, *70*, 9505811. [CrossRef]
3. Keramat, A.; Karney, B.; Ghidaoui, M.S.; Wang, X. Transient-based leak detection in the frequency domain considering fluid–structure interaction and viscoelasticity. *Mech. Syst. Signal Process.* **2021**, *153*, 107500. [CrossRef]
4. Wang, W.; Sun, H.; Guo, J.; Lao, L.; Wu, S.; Zhang, J. Experimental study on water pipeline leak using In-Pipe acoustic signal analysis and artificial neural network prediction. *Meas. J. Int. Meas. Confed.* **2021**, *186*, 110094. [CrossRef]
5. Guo, C.; Shi, K.; Chu, X. Cross-correlation analysis of multiple fibre optic hydrophones for water pipeline leakage detection. *Int. J. Environ. Sci. Technol.* **2022**, *19*, 197–208. [CrossRef]
6. Kothandaraman, M.; Law, Z.; Ezra, M.A.G.; Pua, C.; Rajasekaran, U. Water Pipeline Leak Measurement Using Wavelet Packet-based Adaptive ICA. *Water Resour. Manag.* **2022**, *36*, 1973–1989. [CrossRef]
7. Jiang, W.; Du, L.; Luo, Z.; Wang, Z.; Song, H. Impact localization with a weighted spectral cross correlation method. *Aerosp. Sci. Technol.* **2022**, *126*, 107591. [CrossRef]
8. Trutié-Carrero, E.; Valdés-Santiago, D.; León-Mecías, Á.; Ra, J. Burst detection and localization using discrete wavelet transform and cross-correlation. *RIAI—Rev. Iberoam. Autom. e Inform. Ind.* **2018**, *15*, 211–216. [CrossRef]
9. Martini, A.; Troncossi, M.; Rivola, A. Vibration Monitoring as a Tool for Leak Detection in Water Distribution Networks. In: Ciri Din. 2014, p. 1. Available online: http://www.scopus.com/inward/record.url?eid=2-s2.0-84937219271&partnerID=tZOtx3y1 (accessed on 1 January 2023).
10. Trutié-Carrero, E.; Cabrera-Hernández, Y.; Hernández-González, A.; Ramírez-Beltrán, J. Automatic detection of burst in water distribution systems by Lipschitz exponent and Wavelet correlation criterion. *Meas. J. Int. Meas. Confed.* **2020**, *151*, 107195. [CrossRef]
11. Rathnayaka, S.; Shannon, B.; Rajeev, P.; Kodikara, J. Monitoring of pressure transients in water supply networks. *Water Resour. Manag.* **2015**, *30*, 471–485. [CrossRef]
12. Ravisangar, V.; Charles, T. Special considerations for protecting very long transmission mains from hydraulic transients. In *Pipelines 2011 A Sound Conduit for Sharing Solutions*; ASCE: Reston, VA, USA, 2011; pp. 1215–1224. [CrossRef]
13. Kumar, D.; Tu, D.; Zhu, N.; Shah, R.A.; Hou, D.; Zhang, H. The free-swimming device leakage detection in plastic water-filled pipes through tuning the wavelet transform to the underwater acoustic signals. *Water* **2017**, *9*, 731. [CrossRef]
14. Ayala, P.; Brennan, M.; Almeida, F.; Kroll, F.; Obata, D.; Tabone, A. Vibroacoustic characteristics of leak noise in buried water pipes in Brazil. In Proceedings of the I Jornada Peruana Internacional de Investigación en Ingeniería, Lima, Peru, 11–13 January 2017.
15. Butterfield, J.D.; Krynkin, A.; Collins, R.P.; Beck, S.B.M. Experimental investigation into vibro-acoustic emission signal processing techniques to quantify leak flow rate in plastic water distribution pipes. *Appl. Acoust.* **2017**, *119*, 146–155. [CrossRef]
16. Butterfield, J.D.; Collins, R.P.; Beck, S.B.M. Influence of Pipe Material on the Transmission of Vibroacoustic Leak Signals in Real Complex Water Distribution Systems: Case Study. *J. Pipeline Syst. Eng. Pract.* **2018**, *9*, 05018003. [CrossRef]
17. Gao, Y.; Liu, Y.; Ma, Y.; Cheng, X.; Yang, J. Application of the differentiation process into the correlation-based leak detection in urban pipeline networks. *Mech. Syst. Signal Process.* **2018**, *112*, 251–264. [CrossRef]
18. Trutié-Carrero, E.; Delgado-Hernández, L.A.; González-Zamora, C.; Ramírez-Beltrán, J. Detección y localización de fuga de fondo en tuberías plásticas de agua bajo un ambiente ruidoso. *Rev. Ing. Electrón. Autom. Comun.* **2019**, *40*, 1–15.
19. Kassab, S.; Michel, F.; Maxit, L. Water experiment for assessing vibroacoustic beamforming gain for acoustic leak detection in a sodium-heated steam generator. *Mech. Syst. Signal Process.* **2019**, *134*, 106332. [CrossRef]
20. Xue, Z.; Tao, L.; Fuchun, J.; Riehle, E.; Xiang, H.; Bowen, N.; Prasad, R. Application of acoustic intelligent leak detection in an urban water supply pipe network. *J. Water Supply Res. Technol.—AQUA* **2020**, *69*, 512–520. [CrossRef]
21. Cody, R.A.; Dey, P.; Narasimhan, S. Linear Prediction for Leak Detection in Water Distribution Networks. *J. Pipeline Syst. Eng. Pract.* **2020**, *11*, 04019043. [CrossRef]
22. Gao, L.; Li, D.; Yao, L.; Gao, Y. Sensor drift fault diagnosis for chiller system using deep recurrent canonical correlation analysis and k-nearest neighbor classifier. *ISA Trans.* **2022**, *122*, 232–246. [CrossRef]
23. Liu, Z.; Fang, L.; Jiang, D.; Qu, R. A Machine-Learning-Based Fault Diagnosis Method With Adaptive Secondary Sampling for Multiphase Drive Systems. *IEEE Trans. Power Electron.* **2022**, *37*, 8767–8772. [CrossRef]
24. Chen, B.; Cheng, Y.; Zhang, W.; Mei, G. Investigation on enhanced mathematical morphological operators for bearing fault feature extraction. *ISA Trans.* **2022**, *126*, 440–459. [CrossRef] [PubMed]
25. Oppenheim, A.V.; Schafer, R.W. *Digital Signal Processing*; Research supported by the Massachusetts Institute of Technology, Bell Telephone Laboratories, and Guggenheim Foundation, Englewood Cliffs, N.J.; Prentice-Hall, Inc.: Hoboken, NJ, USA, 1975; p. 598.
26. Gao, Y.; Brennan, M.J.; Joseph, P.F. On the effects of reflections on time delay estimation for leak detection in buried plastic water pipes. *J. Sound Vib.* **2009**, *325*, 649–663. [CrossRef]
27. Li, S.; Cai, M.; Han, M.; Dai, Z. Noise Reduction Based on CEEMDAN-ICA and Cross-Spectral Analysis for Leak Location in Water-supply Pipelines. *IEEE Sens. J.* **2022**, *22*, 13030–13042. [CrossRef]

28. Wen, H.; Zhang, L.; Sinha, J. Adaptive Band Extraction Based on Low Rank Approximated Nonnegative Tucker Decomposition for Anti-Friction Bearing Faults Diagnosis Using Measured Vibration Data. *Machines* **2022**, *10*, 694. [CrossRef]

29. Wang, Z.; Yang, J.; Li, H.; Zhen, D.; Gu, F.; Ball, A. Improved cyclostationary analysis method based on TKEO and its application on the faults diagnosis of induction motors. *ISA Trans.* **2022**, *128*, 513–530. [CrossRef]

30. Medina, R.; Garrido, M. Improving impact-echo method by using cross-spectral density. *J. Sound Vib.* **2007**, *304*, 769–778. [CrossRef]

31. Manolakis, D.G.; Ingle, V.K.; Kogon, S.M. *Spectral Estimation, Signal Modeling, Adaptive Filtering, and Array Processing*; ARTECH HOUSE: Boston, MA, USA, 2005.

32. Chen, B.; Cheng, Y.; Zhang, W.; Gu, F. Enhanced bearing fault diagnosis using integral envelope spectrum from spectral coherence normalized with feature energy. *Meas. J. Int. Meas. Confed.* **2022**, *189*, 110448. [CrossRef]

33. Zhang, B.; Miao, Y.; Lin, J.; Li, H. Weighted envelope spectrum based on the spectral coherence for bearing diagnosis. *ISA Trans.* **2022**, *123*, 398–412. [CrossRef]

34. Allemang, R.J.; Patwardhan, R.S.; Kolluri, M.M.; Phillips, A.W. Frequency response function estimation techniques and the corresponding coherence functions: A review and update. *Mech. Syst. Signal Process.* **2022**, *162*, 108100. [CrossRef]

35. Dragos, K.; Magalhães, F.; Manolis, G.D.; Smarsly, K. Cross-Spectrum-Based Synchronization of Structural Health Monitoring Data. In *European Workshop on Structural Health Monitoring: EWSHM 2022-Volume 2*; Springer: Cham, Switzerland, 2023; pp. 927–936. [CrossRef]

36. Kyophilavong, P.; Abakah, E.J.A.; Tiwari, A.K. Cross-spectral coherence and co-movement between WTI oil price and exchange rate of Thai Baht. *Resour. Policy* **2023**, *80*, 103160. [CrossRef]

37. Bo, T.L.; Li, F. Multi-scale characteristics of the spatial distribution of space charge density that determines the vertical electric field during dust storms. *Granul. Matter.* **2023**, *25*, 6. [CrossRef]

38. Grinsted, A.; Moore, J.C.; Jevrejeva, S. Application of the cross wavelet transform and wavelet coherence to geophysical time series. *Nonlinear Process. Geophys.* **2004**, *11*, 561–566. [CrossRef]

39. Olanrewaju, V.O.; Adebayo, T.S.; Akinsola, G.D.; Odugbesan, J.A. Determinants of Environmental Degradation in Thailand: Empirical Evidence from ARDL and Wavelet Coherence Approaches. *Pollution* **2021**, *7*, 181–196. [CrossRef]

40. Mohammadzadeh, L.; Latifi, H.; Khaksar, S.; Feiz, M.S.; Motamedi, F.; Asadollahi, A.; Ezzatpour, M. Measuring the Frequency-Specific Functional Connectivity Using Wavelet Coherence Analysis in Stroke Rats Based on Intrinsic Signals. *Sci. Rep.* **2020**, *10*, 9429. [CrossRef] [PubMed]

41. Gao, Z.; Lin, J.; Wang, X.; Liao, Y. Grinding Burn Detection Based on Cross Wavelet and Wavelet Coherence Analysis by Acoustic Emission Signal. *Chin. J. Mech. Eng.* **2019**, *32*, 68. [CrossRef]

42. Carrera-Avendaño, E.; Urquiza-Beltrán, G.; Trutié-Carrero, E.; Nieto-Jalil, J.M.; Carrillo-Pereyra, C.; Seuret-Jiménez, D. Detection of crankshaft faults by means of a modified Welch-Bartlett periodogram. *Eng. Fail. Anal.* **2022**, *132*, 105938. [CrossRef]